

Source localization of ictal epileptic activity investigated by high resolution EEG and validated by SEEG

Laurent Koessler^{a,b,c,*}, Christian Benar^{a,b}, Louis Maillard^{c,d}, Jean-Michel Badier^{a,b}, Jean Pierre Vignal^{c,d}, Fabrice Bartolomei^{a,b,e}, Patrick Chauvel^{a,b,e}, Martine Gavaret^{a,b,e}

^a INSERM, UMR751, Marseille, F-13000, France

^b Aix Marseille Université, Faculté de Médecine, Marseille, F-13000, France

^c Centre de Recherche en Automatique de Nancy, Nancy-Université, CNRS, Nancy, F-54000, France

^d CHU Nancy, Service de Neurologie, Nancy, F-54000, France

^e Assistance Publique Hôpitaux de Marseille, Hôpital de la Timone, Service de Neurophysiologie Clinique, Marseille, F-13000, France

ARTICLE INFO

Article history:

Received 28 October 2009

Revised 5 January 2010

Accepted 23 February 2010

Available online 4 March 2010

Keywords:

Source localization

High resolution EEG

Depth EEG

Seizure

Epileptogenic zone

ABSTRACT

High resolution electroencephalography (HR-EEG) combined with source localization methods has mainly been used to study interictal spikes and there have been few studies comparing source localization of scalp ictal patterns with depth EEG. To address this issue, 10 patients with four different scalp ictal patterns (ictal spikes, rhythmic activity, paroxysmal fast activity, obscured) were investigated by both HR-EEG and stereoelectroencephalography (SEEG). Sixty-four scalp-EEG sensors and a sampling rate of 1 kHz were used to record scalp ictal patterns. Five different source models (moving dipole, rotating dipole, MUSIC, LORETA, and sLORETA) were used in order to perform source localization. Seven to 10 intracerebral electrodes were implanted during SEEG investigations. For each source model, the concordance between ictal source localization and epileptogenic zone defined by SEEG was assessed. Results were considered to agree if they localized in the same sublobar area as defined by a trained epileptologist. Across the study population, the best concordance between source localization methods and SEEG (9/10) was obtained with equivalent current dipole modeling. MUSIC and LORETA had a concordance of 7/10 whereas sLORETA had a concordance of only 5/10. Four of our patients classified into different groups (ictal spikes, paroxysmal fast activity, obscured) had complete concordance between source localization methods and SEEG. A high signal to noise ratio, a short time window of analysis (<1 s) and bandpass filtering around the frequency of rhythmic activity allowed improvement of the source localization results. A high level of agreement between source localization methods and SEEG can be obtained for ictal spike patterns and for scalp-EEG paroxysmal fast activities whereas scalp rhythmic discharges can be accurately localized but originated from seizure propagation network.

© 2010 Elsevier Inc. All rights reserved.

Introduction

Source localization techniques have been widely studied and validated for the study of interictal activity (Ebersole, 2000; Lantz et al., 2003; Michel et al., 2004a,b; Gavaret et al., 2004, 2006, 2009). However, there have been few studies concerning ictal source localization (Lantz et al., 2001; Boon et al., 2002; Holmes et al., 2004; Beniczky et al., 2006; Ding et al., 2007). In addition, the relationship between the “irritative” zone (i.e. presenting interictal discharges) and epileptogenic zone remains poorly investigated (Talairach and Bancaud, 1966).

The small number of publications on this topic is largely due to the difficulty in recording epileptic seizures during high resolution

electroencephalography (HR-EEG). This can be explained by the short recording time, due to demanding technical reasons (high number of sensors, high sampling rate, low impedances, comfort, etc.). Moreover, source modeling of seizures is much more complex than source modeling of spikes because of the low signal to noise ratio of some ictal pattern types, their frequent contamination by muscle artifacts, and propagation. Some studies have compared ictal surface EEG with intracranial EEG data (Assaf and Ebersole, 1997; Lantz et al., 1999, 2001; Foldvary et al., 2001; Merlet and Gotman, 2001; Boon et al., 1997, 2002). Other authors have compared ictal surface EEG with anatomic lesions (Ding et al., 2007), epilepsy surgery (Boon et al., 1997; Lantz et al., 2001), or single photon-emission computed tomography (SPECT) (Mine et al., 1998; Beniczky et al., 2006). Due to poor temporal resolution, metabolic investigations are not suitable to study the temporal dynamics of seizures and cannot be used as a valid reference technique.

* Corresponding author. Centre de Recherche en Automatique de Nancy, Nancy-Université, CNRS, 2 Avenue de la Forêt de Haye, F-54000, France. Fax: +33 383 852 945.
E-mail address: l.koessler@chu-nancy.fr (L. Koessler).

Different types of epilepsy (often temporal) and ictal patterns (mainly theta activity and spikes) were investigated in these studies, mainly using equivalent current dipole (ECD) and multiple signal classification (MUSIC) methods. Few studies (Worrell et al., 2000; Holmes et al., 2004) have used distributed source models (low resolution electromagnetic tomography (LORETA)) to localize ictal patterns. In these studies, the conditions of ictal surface EEG recordings were rarely adequate for source localization because of the low number of electrodes (30–40) or the use of a spherical head model.

Magnetoencephalography (MEG) recordings have been demonstrated to yield localizing information in epilepsy surgery candidates (Stefan et al., 2003; Fischer et al., 2005; Knowlton et al., 2006, 2009). Ictal activities have also been investigated by MEG in a few patients (Sutherling et al., 1987; Stefan et al., 1992; Eliashiv et al., 2002; Tanaka et al., 2009). In these studies, ictal magnetic source imaging was compared with the results of epilepsy surgery, intracranial recordings, and scalp EEGs. The authors concluded that the ictal magnetic source localizations were in close agreement with invasive and noninvasive preoperative studies. MEG ictal studies, like EEG ictal studies, concluded that imaging can help in the placement of invasive electrodes and in surgery planning. Despite fewer ergonomic constraints than MEG recordings (which require head immobility), EEG source localization studies of ictal activity are still rare. To date, no data have been published concerning source localization of ictal patterns in conditions of HR-EEG (at least 64 sensors and a high sampling rate) and few comparative studies exist with intracerebral EEG (Merlet and Gotman, 2001; Boon et al., 2002). Moreover, no study has compared dipolar and distributed source methods. It is also unclear what kind of scalp-EEG ictal patterns permit reliable source localization.

The main purpose of this study was to evaluate the accuracy of ictal source localization in distinct types of scalp-EEG ictal patterns, using stereoelectroencephalography (SEEG) as a validating method. The different source localization methods were also compared.

Methods

Subjects

Ten drug-resistant partial epilepsy patients underwent HR-EEG recording of seizures (six patients were investigated in the Clinical Neurophysiology Department of Timone Hospital, Marseille, and four in the Neurology Department of the University Hospital, Nancy). Each patient gave his informed consent and the study was approved by the ethics committee (CPP) of Marseille.

Patients first underwent a presurgical evaluation including careful history taking, neurologic examination, video-EEG recording of seizures, anatomic magnetic resonance imaging (MRI), interictal \pm ictal single photon computerized tomography (SPECT), positron-emission tomography (PET), and neuropsychologic evaluation. Because several hypotheses were proposed by the noninvasive investigations, all patients underwent SEEG in order to delineate the epileptogenic zone. In the population overall, four patients had temporal lobe epilepsy (TLE), three had frontal lobe epilepsy (FLE), two had posterior cortex epilepsy (PCE), and one had temporo-perisylvian epilepsy (TPE). Median age at the time of SEEG evaluation was 25 years (range, 12–36 years). The characteristics of the patients are shown in Table 1.

High resolution EEG

Recordings

HR-EEG data were recorded using 64 scalp electrodes (Quickcap; Compumedics Neuroscan, El Paso, TX, USA) in six patients and 64 EEG–MRI sensors taped with collodion (Koessler et al., 2008) in four.

Electrodes were placed according to the 10–10 international system (Oostenveld and Praamstra, 2001). Impedances were all <5 k Ω . The signal was recorded from 1 h to 2 days at a 1 kHz sampling rate. The activity was digitally filtered with a bandpass 0.15–200 Hz which prevents aliasing (SynAmps; Compumedics Neuroscan, Charlotte, NC, USA, or SD64 Headbox; Micromed, Italy). Drug-induced activation or other activation procedures such as hyperventilation were not used.

Scalp-EEG ictal detection, selection and analysis

The initial part of each scalp-EEG seizure was analyzed by a trained epileptologist (MG and LM) using bipolar and monopolar montages. Ictal patterns were classified according to four ictal patterns adapted from the classification proposed by Foldvary et al. (2001): (1) ictal spikes; (2) rhythmic activity; (3) paroxysmal fast activity; and (4) obscured. Ictal spikes were defined by initial transient elements, clearly distinguished from background activity, with pointed peaks, usually repetitive: three or more in a sequence (Chatrian et al., 1974; Foldvary et al., 2001). Ictal rhythmic activity was characterized by alpha, theta or delta frequencies. The third scalp-EEG ictal pattern was characterized by paroxysmal fast activities with rhythmic activities ≥ 13 Hz. The obscured pattern was defined as a pattern evolving from a period obscured by artifacts such that the precise time, pattern, and distribution of onset were indiscernible (Foldvary et al., 2001). For source localization analysis, seizures were divided into several events succeeding in time. Time analysis windows of each event ran from the start to the end of the change in amplitude (i.e. depolarization and repolarization of the EEG signal). For each subject, the signal to noise ratio was determined, defined by dividing the amplitude envelope of the ictal pattern by the amplitude envelope of the background activity. Channels that recorded scalp-EEG ictal patterns with maximal amplitude (dominant channels) were determined with Advanced Signal Analysis (ASA) software (ANT Software, Enschede, The Netherlands) using a common average reference.

Sensor localizations

Two methods were used to localize EEG electrodes. For six patients, the positions of all electrodes and anatomic landmarks (nasion, right and left tragi) were registered with a 3D digitizer system (3Space Fastrak; Polhemus, Colchester, VT, USA). These three marking points were used to define a spatial reference. The patient's forehead and nasal surface were also registered by collecting approximately 600–700 points while moving the digitizer across the head contour. A second method was used for four patients: this consisted of automatic localization and labeling of EEG sensors (ALLES) in the MRI volume (Koessler et al., 2008). For all patients, electrodes were localized in the fiducial system, defined by anatomic landmarks (nasion, right and left tragi).

MRI and head modeling

Three-dimensional MRI was based on a T1-weighted sequence, with a pixel size of 1.25 mm² and slice thickness of 1.25 mm. The same anatomic landmarks (nasion, right and left tragi) were identified on the 3D MRI. Thus, the same spatial reference was defined for neurophysiologic and structural data. The realistic head model was based on a boundary element method, which describes the individual surfaces by triangulation, with about 1700–2000 nodes per model. The segmentation process, identification of the three compartments of isoconductivity (intracranial space, skull, and scalp) was performed with ASA software (ANT Software, Enschede, The Netherlands). Automatic 3D segmentation was used, the skull being the dilatation ($\times 3$) of the intracranial space. Triangulation of the surfaces was performed automatically. Based on these triangulation data, a realistic EEG transfer matrix was calculated. This realistic head model took into consideration individual differences in head volume. Different specific conductivities were attributed to each volume according to Gonçalves

Table 1
Patients' characteristics.

Patients	Gender	Age (y)	Initial ictal symptoms	Anatomical MRI	Histopathology	Localization of epilepsy	SEEG	Scalp-EEG ictal pattern		
								Dominant channels	SNR	Frequency (Hz)
Scalp-EEG ictal pattern: ictal spikes										
1—MC	F	24	Elementary auditory hallucination, auditory illusion, warm sensation	R temporal lesion	Ectopic neurons suggestive of MCD	TLE	X	FT10, T8, TP8	4	<2
2—PE	F	23	Fear, thoracic oppression, loss of contact	R base-temporal FCD	—	TLE	X	T8, TP8, P8	4	<2
3—DT	M	23	Visual illusion, loss of contact, head deviation to the left	R basal temporo-occipital FCD	—	PCE	X	P8, PO8, O2	5	<2
4—JT	M	36	Loss of contact, elevation of the right arm, aversion of the head to the right	L middle cerebral artery territory infarction	Gliosis	FLE	X	F1, Fz, AF3	8	<2
Scalp-EEG ictal pattern: rhythmic activity										
5—PA	F	36	Loss of contact, oral and gestural automatisms	R HS	Gliosis	TLE	X	P8, PO8, O2	1.5	04–05
6—PHA	M	17	Visual blurring, eye and head deviations to the right, loss of contact	R baso-occipital FCD	—	PCE	X	C6, T8, TP8	2	02–03
Scalp-EEG ictal pattern: paroxysmal fast activity										
7—SS	F	27	Dreamy state, warm sensation, loss of contact	R schizencephaly	—	TLE	X	F8, FT8, T8	7	15–20
8—MB	M	17	Grunting, vocalization, tachpnea	Normal	—	FLE	X	FP1, AF3, AF7	1	15–16
Scalp-EEG ictal pattern: obscured										
9—FD	M	12	Extension of the right arm, speech arrest	Normal	—	FLE	X	FP1, FPz, F3 and artifacts	3	—
10—VM	M	34	Fear, thoracic oppression, speech arrest	R frontal cortectomy, L fronto-temporal cortectomy	Cavernoma/Gliosis	Temporo-perisylvian E	X	FP1, AF3, F3 and artifacts	1.5	—

Classification of patients according to their scalp-electroencephalography (EEG) ictal pattern (ictal spikes, rhythmic activity, paroxysmal fast activity, obscured), gender (six males/four females), age at time of SEEG (12–36 years), initial ictal symptoms observed during video-EEG, anatomic magnetic resonance imaging (MRI), histologic diagnosis, and scalp-EEG ictal pattern characteristics: dominant channels, signal to noise ratio and frequency.

FCD: focal cortical dysplasia; FCD indicated in anatomic MRI volume means MRI suggestive of gyral thickening with abnormal MRI signal, usually T2 prolongation in the underlying white matter, according to the criteria of Kuzniecky and Barkovich, 2001; DNET: dysembryoplastic neuroepithelial tumor; HS: MRI suggestive of hippocampal sclerosis (unilateral hippocampal atrophy and increased signal in the medial structures); MCD: mild cortical dysplasia or microdysgenesis; L: left; R: right; E: epilepsy; PC: posterior cortex; TL: temporal lobe; FL: frontal lobe.

et al. (2000) (0.33 S/m for intracranial space and scalp, 0.008 S/m for skull, conductivity ratio (skull/scalp) = 1/40).

SEEG data

SEEG recording

In Marseille hospital, SEEG was performed using multicontact depth electrodes (diameter 0.8 mm, 10–15 contacts, each 2 mm long with an intercontact distance of 1.5 mm) implanted intracerebrally according to Talairach's stereotactic method (Talairach et al., 1974). The precise localization of the target cortical structures was based on surface rendering of the 3D T1-weighted sequence, on 3D MRI reconstruction, and on peroperative telemetric angiography. Seven to 10 electrodes were implanted, providing 70–150 points of measurement in each case, and consequently an extended electrophysiologic sampling of the brain areas of interest. The cortical targets for the positioning of electrodes were determined by the clinical, neurophysiologic, and anatomic characteristics of each patient. The exact position of each depth electrode contact was determined postoperatively using an immediate postoperative computed tomography (CT) scan and MRI performed following electrode removal (3D T1-weighted images and T2-weighted coronal images).

In the Nancy hospital, stereotactic placement of the intracerebral electrodes was performed as follows: a Leksell G-frame (Elekta S.A, Stockholm, Sweden) was positioned on the patient's head and stereotactic MRI (3D SPGR T1-weighted sequence with double

injection of gadolinium) was carried out. MRI was imported into a computer-assisted stereotactic module (Leksell Surgiplan®; Elekta S.A, Stockholm, Sweden), and electrode trajectories were calculated according to preoperative planning, with careful avoidance of vascular structures. A postoperative stereotactic CT-scan was then carried out and fused with preoperative MRI to determine the exact position of each electrode (for a more detailed description, see Maillard et al., 2009). Signals were recorded on a 128-channel Deltamed or Micromed system, with sampling at 512 Hz and recording on a hard disk (16 b/sample) using no digital filter. The only filter present in the acquisition procedure was a hardware analog high-pass filter (cut-off frequency = 0.16 Hz) used to remove very slow variations that sometimes contaminate the baseline.

SEEG analysis

For each implanted depth electrode, EEG recordings were obtained from 15 contacts. The external contacts (numbered 10–15) recorded lateral infolded cortex and gyral crowns. Respectively, the internal contacts (numbered 1–5) recorded the depth medial cortex. For each patient, the same terminology was used to determinate the anatomic position of depth electrodes.

Intracerebral ictal onsets were defined after a consensual analysis by at least two epileptologists (PC, FB, MG in Marseille, and JPV, LM in Nancy). This analysis was made visually on video-SEEG traces in bipolar montage. Intracerebral EEG seizure onsets were delineated by depth electrodes, which recorded the initial modifications of

Table 2

Source localization results.

Patients	SNR	Equivalent current dipole (ECD), RD, MD		MUSIC	LORETA	5-LORETA	Summarized intracerebral epileptogenic zone
		Localization	GOP (%)				
Scalp-EEG ictal pattern: ictal spikes							
1—MC	4	R superior temporal G, R superior temporal S	87—91	R superior temporal G, R superior temporal S	R posterior middle temporal G	B posterior middle temporal G	R superior temporal S
2—PE	4	R anterior temporal	92—97	R anterior temporal	Basal frontal bilateral	R basal frontal	R anterior temporal lobe (medial and lateral)
3—DT	5	Basal part at the R occipito-temporal junction	89—96	Basal part of the R occipito-temporal junction	Basal part of the R temporo-parieto-occipital junction	Bilateral posterior	R anterior and basal temporal lobe, R cuneus, R gyrus lingual
4—JT	8	L sup. and mid. frontal G, anterior part	85—87	L sup. and mid. frontal G, anterior part	L sup. and mid. Frontal gyrus, anterior part	Lateral part of the L frontal lobe	L BA 47—12, L BA 9—46, L BA 6—8
Scalp-EEG ictal pattern: rhythmic activity							
5—PA	1.5	R perisylvian	71—88	Centrencephalic	R lateral temporal	B lateral temporal	R anterior and medial temporal lobe (insular propagations)
6—PHA	2	R temporal lobe	73—85	Anterior part at the R temporal lobe	Basal part at the R occipital lobe	Basal part of the L occipital lobe	R basal occipital lobe (R temporal propagation)
Scalp-EEG ictal pattern: paroxysmal fast activities							
7—SS	7	Anterior and lateral part of the R temporal lobe	89—85	Anterior and lateral part of the R temporal lobe	Anterior and lateral part of the R temporal lobe	Anterior and lateral part of the R temporal lobe	Anterior and lateral part of the R temporal lobe
8—MB	1	R medial orbital gyrus	85—89	L medial orbital gyrus	L lateral orbital gyrus	L medial orbital gyrus	L medial and lateral orbital gyrus
Scalp-EEG ictal pattern: obscured							
9—FD	3	L superior frontal sulcus (MD)	35—70	Medial and basal part of L frontal lobe	Bilateral frontal	Bilateral frontal	L superior frontal sulcus
10—VM	1.5	Basal part of L frontal lobe	43—58	Basal part of L frontal lobe	Medial part of L frontal lobe	Medial part of the L frontal lobe	L frontal lobe (medial/lateral/basal), posterior part of the previous L cortectomy

Source localization results and summarized intracerebral epileptogenic zone for each patient. AR, amplitude ratio; GOF, goodness of fit; R, right; L, Left; G, gyrus; S, sulcus; MUSIC, multiple signal classification; ECD, equivalent current dipole; BA, Brodmann area.

background activity simultaneously (Talairach et al., 1974). Seizure onset is usually characterized by the emergence of rapid discharges (beta-gamma range) in one or several brain regions, and is preceded by “preictal” changes in background activity (preictal spiking, slow waves, etc.) (Bartolomei et al., 2008).

Source localization

For source localization analysis, successive temporal windows were analyzed from the onset of the seizure to a maximum of 3 s later. Seizure onset was defined by visual inspection of both scalp-EEG and patient's semiology. Between 5–10 activities were analyzed per seizure. Each activity lasted from a few milliseconds in the case of ictal spikes to 1 s in the case of paroxysmal fast activity and rhythmic activity group. The source localizations of one ictal activity defined by a time window were illustrated.

ECD

For all subjects, single unconstrained equivalent current dipole modeling was carried out on all different scalp-EEG seizures. This analysis was first performed with a moving dipole approach (i.e. calculation of a new dipole localization, orientation, and amplitude for each millisecond). This allows determination of whether a particular area can be identified as the origin of the activity when the localization of the equivalent current dipole remains stable in the same area for sufficient time (20–30 ms). Apparent movement of the dipole between distant structures reveals an inadequate source model or propagation of the activity; unstable localization can also appear in the case of insufficient signal to noise ratio. For a moving dipole, its position characterized by a maximal value of goodness of fit (percentage of EEG data that could be explained by the model) was retained. No dipole confidence volume was measured but, as described by Fuchs et al. (2004), the size of the axes of the confidence ellipsoids is inversely proportional to the SNR of the measured data.

Thus, the confidence volume is inversely proportional to the third power of the SNR. At last, a spatio-temporal model (single unconstrained rotating dipole) (i.e. same localization within the time window) was also used (Scherg, 1990). Localization was stable during the time window whereas orientation and amplitude were estimated for each millisecond. No noise floor regularization was done with ECD models. Noise was estimated by the SNR ratio (see Table 1). Reliability of ECD models (goodness of fit) has to be considered according to this ratio.

Table 3

Concordance between source localization methods and SEEG.

	Concordance between source localization and SEEG			
	ECD	MUSIC	LORETA	sLORETA
<i>Scalp-EEG ictal pattern: ictal spikes</i>				
1–MC	Yes	Yes	No	No
2–PE	Yes	Yes	No	No
3–DT	Yes	Yes	Yes	No
4–iT	Yes	Yes	Yes	Yes
<i>Scalp-EEG ictal pattern: rhythmic activity</i>				
5–PA	Yes	No	Yes	Yes
6–PHA	No	No	Yes	No
<i>Scalp-EEG ictal pattern: paroxysmal fast activity</i>				
7–SS	Yes	Yes	Yes	Yes
8–MB	Yes	Yes	Yes	Yes
<i>Scalp-EEG ictal pattern: obscured</i>				
9–FD	Yes	No	No	No
10–VM	Yes	Yes	Yes	Yes

Concordance between source localization methods and SEEG for the anatomical localization of epileptogenic zone. Yes indicates that there is an anatomical congruence between SEEG and source localization method.

MUSIC

The MUSIC method was used to get an estimation of the number and location of generators within the intracranial volume. This method was

adapted from a subspace scanning technique used in radar technology (Schmidt, 1986). The method is based on eigenvector decomposition of the data. Eigenvectors are then separated into signal subspace and noise

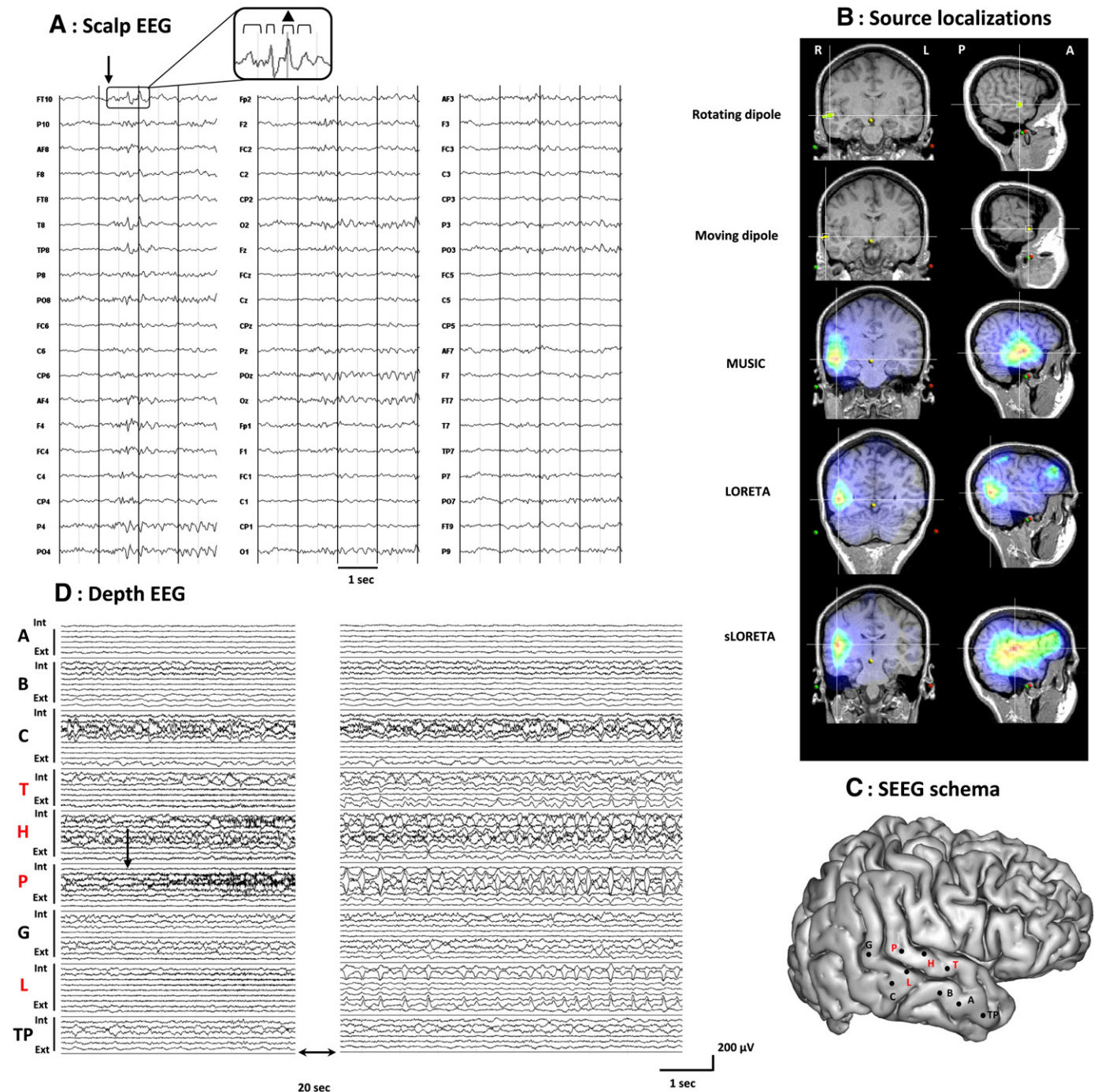


Fig. 1. Scalp and depth electroencephalography (EEG), source localization, and stereo electroencephalography (SEEG) schema for patient 1 (ictal spike group). (A) Scalp-EEG ictal pattern was recorded over the right anterior and middle temporal regions, dominant channels were FT8, FT10, T8 and TP8 (monopolar montage, common average reference). Scalp seizure onset is indicated with an arrow. Source localization methods were performed on all events marked with a brace. Source localizations were obtained for the temporal window marked with a triangle. (B) Ictal source localizations in frontal and sagittal views, with rotating dipole, moving dipole, MUSIC, LORETA and sLORETA localizations. Equivalent current dipole (ECD) and MUSIC were localized in the anterior part of the right superior temporal gyrus whereas distributed source models were localized in the right posterior middle temporal gyrus. Source localizations were reproducible for all temporal windows. (C) SEEG schema, superimposed on patient's 3D magnetic resonance image, performed using nine depth electrodes in the right hemisphere, recordings as follows (medial and lateral contacts): B, hippocampal head/middle temporal gyrus; A, amygdala/middle temporal gyrus; TP, temporal pole; C, hippocampal tail/posterior middle temporal gyrus; H, insula/Heschl gyrus; T, insula/anterior part of superior temporal gyrus; P, planum temporale (median and external contacts); L, posterior part of the superior temporal sulcus (median and external contacts); G, posterior cingulate gyrus/supramarginalis gyrus. (D) Fast low-voltage discharge was recorded by the four depth electrodes exploring the superior temporal gyrus and superior temporal sulcus. Several seconds later, depth ictal spikes were recorded (electrodes L, P, H, and T) (seizure onset is indicated with an arrow). Source localizations were concordant with the second part of this seizure. The initial more medial fast discharge (medial leads of depth electrode P) was unobserved on ictal scalp-EEG.

subspace (Mosher et al., 1999). The signal subspace was defined as the eigenvectors explaining at least 95% of the signal.

Noise floor regularization was done using the PCA decomposition on the time window of analysis and the selection of the signal subspace. The whole brain volume is scanned to find the sources that most contribute to the signal subspace. A grid is built with n equidistant (10 mm) equivalent current dipoles. The peaks of the scan correspond to the putative positions of equivalent dipoles. For a given seizure, each successive activity was analyzed. The localization, which is the peak with the highest metric of MUSIC, was illustrated.

Distributed source model (LORETA and sLORETA)

Distributed source models were also used to study ictal patterns. These models do not require a number of sources. They are based on reconstruction of brain electric activity at each point on a 3D grid (space of 10 mm) of solution points. Each solution point is considered as a possible location of a current source. Solving the inverse problem with a distributed source model needs constraints (anatomic and/or mathematical), which can vary from one model to another. The Laplacian weighted minimum norm algorithm (LORETA; Pascual-Marqui et al., 1994) was used. This source model is based on a physiologic constraint that selects the solution with a smooth spatial distribution by minimizing the Laplacian of the weighted sources. The underlying assumption is that neighboring grid points are more likely to have a similar orientation and activation strength than distant grid points (Pascual-Marqui et al., 1994). Standardized low resolution electromagnetic tomography (sLORETA) was also used (Pascual-Marqui, 2002). This approach hypothesizes that the noise present in the measured signal is the main source of uncertainties and errors in the activity estimated by noninvasive imaging techniques. sLORETA standardizes the estimated signal to the noise sensitivity at each spatial location. This results in a statistical map. In our study, all time points were analyzed and the source with the highest amplitude across time and space was chosen. In case of LORETA and sLORETA, we used the interval window for which we computed the inverse solution to estimate the noise floor. For these methods, noise was assumed to be independent in each sensor. Only the standard deviation was thus specified. This was done using a regularization parameter. In our study, regularization was estimated via Generalized Cross Validation based on a leave one out method (Pascual-Marqui, 2002; Trujillo-Barreto et al., 2004).

Concordance between ictal source localizations and SEEG

For each method described, the concordance between ictal source localization and epileptogenic zone defined by SEEG was determined. Results were considered to be congruent if they located in the same sublobar area as defined by a trained epileptologist (MG, LM, and FB).

Results were considered discordant if they were located in different lobes or were separated by a major anatomic fissure or sulcus (Tables 2 and 3). For each method, the ratio obtained for the 10 patients investigated by HR-EEG and SEEG was computed.

Results

Patient classification according to scalp-EEG ictal pattern

For each patient, ictal source localizations were compared with the intracerebral epileptogenic zone as determined by SEEG. In the ictal spike group (four patients), signal to noise ratios ranged from 4–8 (Table 1), and spiking frequency was <2 Hz. In the rhythmic activity group, one patient had TLE and one had PCE; signal to noise ratios ranged from 1.5–2. Rhythmic frequencies were in the delta and theta bands. In the paroxysmal fast activity group, one patient had TLE and one had FLE; signal to noise ratios ranged from 1–7. In the obscured

group (two patients), signal to noise ratios ranged from 1.5–3. In this group, one patient had FLE and one had TPE.

Ictal source localizations

Scalp-EEG ictal spikes

Four patients were classified in this group (patients 1–4): two had TLE, one had PCE, and one had FLE. The dominant channels of ictal spikes were temporal channels in two patients (patients 1 and 2), frontal channels in one (patient 4), and occipito-temporal channels in one (patient 3). The characteristics of these ictal spikes are shown in Table 1. In this group, goodness of fit values ranged from 87–97%. In all cases, ECD and MUSIC are located in the same area as the epileptogenic zone defined by SEEG (Table 2). Distributed source models were concordant with intracerebral data in two of four cases (patients 3 and 4 for LORETA, and only patient 4 for sLORETA). The data for patient 1, who is representative, are illustrated in Fig. 1 (see also Supplementary Fig. S1).

Scalp-EEG rhythmic activity

Two patients were classified in this group (patients 5 and 6): one had TLE and one had PCE. Rhythmic activities were recorded in the posterior area for one patient (patient 5) and in the temporal area for one (patient 6). Signal to noise ratios ranged from 1.5–2 (Table 1) and rhythmic frequencies were in the delta and theta bands (2–5 Hz). Goodness of fit values ranged from 71–88%. The detailed characteristics of these rhythmic activities are shown in Table 1. Source localization of rhythmic patterns was performed with a bandpass filter around the discharging frequency. Rhythmic discharges were analyzed with a time window comprised between 100 ms and 1 s. LORETA was concordant with intracerebral data while MUSIC was not (Table 2). The data for patient 5, who is representative, are illustrated in Fig. 2 (see also Supplementary Fig. S2).

Scalp-EEG paroxysmal fast activity

Two patients were classified in this group (patient 7 had TLE, and patient 8 had FLE). Paroxysmal fast activity was recorded in the temporal area for patient 7 and in the fronto-polar region for patient 8. Signal to noise ratio was equal to 7 for patient 7 and 1 for patient 8. Goodness of fit values ranged from 85–95%. Source localizations for patient 7 were in the anterior and lateral part of the right temporal lobe and for patient 8 in the left medial and lateral orbital gyrus. Source localizations for these two patients were congruent with the epileptogenic zones defined by intracerebral investigations (Table 2). The data for patient 7 are shown in Fig. 3 (see also Supplementary Fig. S3).

Obscured activity

Two patients were classified in this group (patient 9 had FLE and patient 10 had TPE). For both patients, ictal activity was recorded in the frontal area. Despite no clear beginning of the ictal discharge and abundant muscle artifacts, attempts were made to select the initial scalp-EEG ictal event. For these two patients, there was a rhythmic discharge masked by the artifacts, with a frequency of 2–3 Hz for patient 9 and 10–20 Hz for patient 10. In order to enhance the signal to noise ratio and eliminate muscle artifacts, a bandpass filter was applied around the discharge frequency. This group was characterized by low goodness of fit values (range, 35–70%). For patient 9, only the moving dipole was concordant with the epileptogenic zone defined by intracerebral investigations. For patient 10, all source localization methods were, however, concordant with the epileptogenic zone (Table 2).

Concordance between ictal source localizations and SEEG

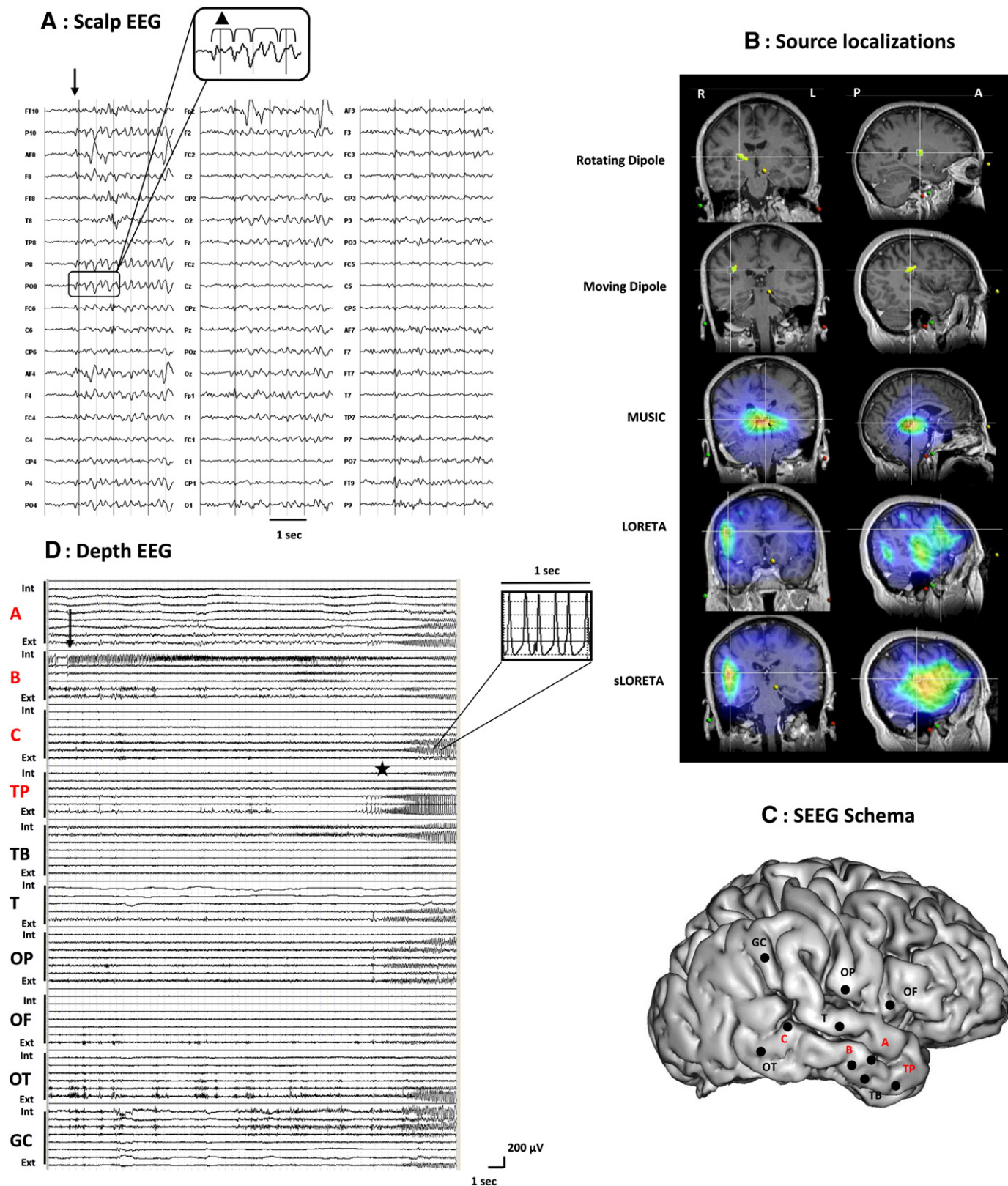
All patients were investigated by both HR-EEG and SEEG. Source localization methods could be applied in all patients. In each patient, at least one method yielded a localization consistent with the epileptogenic zone as defined by SEEG. The best concordance between

source localization methods and SEEG was obtained with the ECD method (9/10). MUSIC and LORETA had a concordance with SEEG of (7/10), whereas sLORETA had a concordance of 5/10 (Table 3). In our population, four patients (patients 4, 7, 8, 10) had 100% concordance between all source localization methods and SEEG. These patients were characterized by distinct types of partial epilepsies and distinct

scalp-EEG ictal patterns. Signal to noise ratio was high for only some of them.

Dynamic analysis of seizures

Stability of all source localizations was observed for all patients. Stability was analyzed during the temporal window of each pattern



and for each successive pattern of the seizures. The first observation was the reproducibility of source localization during the temporal window of analysis. This was the most frequently observed situation, particularly in the ictal spikes, rhythmic activity and obscured groups. Very stable source localization was noticed during the middle of the temporal window, which correspond to maximal amplitude (maximal signal to noise ratio) of the pattern. One hypothesis for the stability of source localization was that the timescale of seizure propagation was much larger than the temporal window of analysis. The second observation was the displacement of the source model during the temporal window of analysis. For only one patient (patient 7), a posterior to anterior implication of the source model was observed during the time window. The same displacement was observed with both dipolar and distributed source models. Movements of the sources were limited in the epileptogenic network defined by SEEG. This displacement allowed the identification of the complete epileptogenic network identified by SEEG (anterior and medio-lateral part of the right temporal lobe).

Reproducibility of source localization was noted for successive patterns of seizures. This was observed during the first 3 s of the seizures and for different types of successive pattern. Reproducibility of source localization was observed for all types of source models (dipolar and distributed).

Discussion

The main objective of this study was to determine the best conditions for locating the epileptogenic zone with HR-EEG in distinct types of scalp-EEG ictal patterns, using SEEG as a validating method. Simultaneous EEG–SEEG recordings would be the best validation method for this kind of study. However, surgical constraints of SEEG (asepsis, presence of guiding screws ...) did not allow using a high number of scalp-EEG sensors.

Ten drug-resistant partial epilepsy patients who underwent HR-EEG and subsequent SEEG were investigated. All types of scalp ictal patterns can be analyzed and accurately localized with HR-EEG. Agreement with HR-EEG and SEEG was 9/10 for ECD, 7/10 for MUSIC and LORETA, and 5/10 for sLORETA. In all types of scalp-EEG patterns (ictal spikes, rhythmic discharge, paroxysmal fast activity, obscured) an accurate localization could be obtained. In our population, at least one source localization method gave a concordant result with intracerebral investigations.

Ictal spikes

In this group, ECD and MUSIC were always consistent with intracerebral investigations while only 3/8 concordance was found for distributed source models. The low level of agreement between distributed sources and SEEG reflects two distinct situations: localizations lying in the vicinity of the epileptogenic zone defined by SEEG in two patients (patient 1 with source localizations in the right middle gyrus instead of the right superior temporal gyrus, and patient 2 with source localizations in the right basal frontal region

instead of the right anterior temporal lobe), and bilateral solutions in patient 3. These errors in source localization could result from the short duration of the analyzed spikes which did not allow the noise in the signal to be extracted correctly during the time window. Moreover, distributed source models were more appropriate to localize a widespread epileptogenic zone (patient 4) than a focal epileptogenic zone (patients 1–3). For focal depth sources, it is possible that distributed source models give two superficial bilateral sources rather than one deep source.

At the difference of interictal phases, ictal spikes are rare and cannot be averaged to enhance signal to noise ratio. In our study, ictal spikes had a high amplitude ratio and presented a focal scalp electric field. An accurate localization could be obtained with ECD and MUSIC in all types of epilepsy studied (TLE, FLE, and PCE). The adequacy of these two models has been demonstrated previously for source localization of interictal spikes (Ebersole, 2000; Lantz et al., 2003; Michel et al., 2004a,b; Gavaret et al., 2004, 2006, 2009) and ictal spikes (Ebersole, 2000; Mine et al., 2005). In 2000, Ebersole et al. demonstrated that dipole orientation could provide information about the origin of temporal lobe seizures. The same conclusion was reached by Mine et al., in 2005 with realistic head models. Taken together, these data strongly suggest that ictal spikes are good candidates for source localization with ECD and MUSIC.

To summarize, a high level of agreement between source localization methods and SEEG can be obtained with ictal spikes. One explanation for this result is that some ictal spikes reflect neocortical onset seizures (Azar et al., 2009) and it therefore appears that source localization can accurately identify neocortical activity.

Rhythmic activity

In this group, two patients (patient 5 with TLE and patient 6 with PCE) were investigated. For patient 5, source localizations were concordant with one part of the epileptogenic zone (i.e. localized in the right perisylvian area). Indeed, intracerebral ictal patterns started with low-voltage fast activity in the anterior hippocampus followed by rhythmic activity in the insular area. ECD and distributed source models gave accurate source localization of the second part of the intracerebral discharge. It has been proposed that partial seizures in the brain are generated by a first set of structures called the “epileptogenic zone network” generating rapid discharges. A second set of structures are involved later (“propagation network”) in which activities are slower, culminating in the theta range (Bartolomei et al., 2008). These results show that source localization is efficient to localize the regions involved in the propagation networks affecting large cortical areas. For patient 6, only LORETA disclosed source localizations concordant with the epileptogenic zone (i.e. localized in the basal part of the right occipital lobe).

It is noteworthy that all our analyses were performed with bandpass filtering around the frequency of the discharge. This technique improves source localization because it reduces artifacts, which decrease the signal to noise ratio (Lantz et al., 1999). Several other signal treatment methods have been reported to improve the

Fig. 2. Scalp and depth electroencephalography (EEG), source localization, and stereoelectroencephalography (SEEG) schema for patient 5 (rhythmic activity group). (A) Scalp-EEG rhythmic activity was recorded over the right parieto-occipital region, the maximum amplitude being on channels P8 and PO8 (monopolar montage, common average reference). In the initial part, the frequency of this rhythmic activity was 4–5 Hz. Scalp seizure onset is indicated with an arrow. Source localization methods were done on all events marked with a brace. (B) Ictal source localizations corresponding to the temporal window marked with a triangle, in frontal and sagittal views, using rotating dipole (RD), moving dipole (MD), MUSIC, LORETA and sLORETA. Equivalent current dipole (ECD) was located in the right perisylvian region. MUSIC was centrencephalic. LORETA and sLORETA source localizations were large, being localized in the right lateral temporal and perisylvian areas. Source localizations were reproducible for all temporal windows. (C) SEEG schema, superimposed on patient's 3D magnetic resonance image, was performed using 10 depth electrodes in the right hemisphere, recordings as follows (medial and lateral contacts): B, hippocampal head/middle temporal gyrus; A, amygdala/middle temporal gyrus; TP, internal and lateral temporal pole; C, hippocampal tail/middle temporal gyrus; TB, parahippocampal gyrus/temporo-basal area; T, insula/superior temporal gyrus; OP, insula/parietal operculum; OF, insula/frontal operculum; OT, occipito-temporal junction; GC, posterior cingulate gyrus/supramarginalis gyrus. (D) Depth seizure involved, for the first 15 s, the medial contacts of electrode B (seizure onset is indicated with an arrow). Several seconds later (indicated by a star), the seizure spread to the lateral contacts of depth electrodes A, B, C, TP, T, OP, OT, and the medial and lateral contacts of electrode GC. At this time, frequency of this depth rhythmic discharge was the same as the rhythmic discharge recorded on the surface (4–5 Hz). Thus, ECD, LORETA, and sLORETA source localizations were concordant with the second part of this seizure: rhythmic propagation to the whole lateral temporal and perisylvian cortex.

quality of localization. Autoregressive modeling (Fraszczuk et al., 1994), time-frequency analysis (Fraszczuk et al., 1998; Osorio et al., 1998), wavelet analysis (Unser and Aldroubi, 1996), and methods related to nonlinear dynamics (Bullmore et al., 1994; Lehnertz and Elger, 1995) have been used for the analysis of ictal EEG in intracranial, surface, or combined intracranial and surface recordings. Fourier spectral analysis, which is the basis of the Fast Fourier Transform (FFT) dipole approximation method (Michel et al., 1992), has also been used in recent investigations to analyze surface recorded epileptic seizures of mesiotemporal origin (Lantz et al., 1999, 2001; Blanke et al., 2000). It is now well known that epileptic seizures are characterized by changes in the frequency domain (Hilfiker and Egli, 1992). Thus, ictal activity can be better studied with frequency filtering to avoid background activity analysis.

To summarize, rhythmic discharges could often be localized because they originated from large neocortical areas and had sufficiently high amplitude to produce scalp EEG. In our study, scalp rhythmic discharges always originated from the propagation network of the epilepsy seizure. This propagation zone can be accurately localized at the difference of the medial temporal epileptogenic zone that produces no visible electrical field on scalp EEG.

Paroxysmal fast activity

Due to the high skull resistivity and to the distance between the cortical generator and the sensors, low-voltage fast activity is often overshadowed by background EEG activity. This overshadow is only due to the attenuation of the amplitude of the fast activity. As described by Oostendorp et al., 2000, the skull conductivity is constant for frequencies under 10 kHz.

For patient 7 (with TLE), fast activity originated from the lateral part of the anatomic lesion (i.e. schizencephaly) and for patient 8, fast activity originated from the lateral and medial part of the left orbital gyrus. For patient 7, the signal to noise ratio of this ictal pattern was very high whereas for patient 8 the signal to noise ratio was equal to one. However in these two cases, source localizations were associated with excellent goodness of fit. All source localizations were concordant with SEEG (i.e. localized in the anterior and lateral part of the right temporal lobe for patient 7 and the left medial and lateral orbital gyrus for patient 8). Dipolar and distributed source models gave the same localizations. No bandpass filter was needed to perform source localization for patient 7. Conversely, for patient 8, signal preprocessing was required to extract the paroxysmal fast activity. Baseline correction, wavelet analysis and bandpass filtering were thus performed.

For these patients, the depth ictal pattern was similar to the pattern recorded on the scalp. The only change in the scalp pattern was the decrease in signal amplitude. Ictal patterns were characterized by a fast oscillation (15–20 Hz) followed by a long negative wave for patient 7 and by fast low-voltage activity for patient 8. For patient 7, source localization methods were excellent at identifying which part of the anatomic lesion was responsible for the ictal pattern.

Source localization methods, as well as SEEG, allowed definition of the posterior limit of the cortectomy. For patient 7, the discharge was very spike-like. So the same advantages as the ictal spike group can be observed on the reliability and the precision of source localizations.

To summarize, our data strongly support that scalp-EEG paroxysmal fast activity reflects proximity between the epileptogenic zone and the recording electrodes (Foldvary et al., 2001). When fast low-voltage activity originated from depth structures (patients 1 and 5), it was not visible on scalp EEG.

Obscured pattern

Two patients were included in this group (patient 9 with FLE and patient 10 with TPE). This was defined by a pattern evolving from a period obscured by artifacts such that the precise time, pattern and distribution of onset were indiscernible (Foldvary et al., 2001). In this study, scalp ictal patterns were recorded in the frontopolar area. The principal source of artifacts in this group was muscular activity. Rhythmic activities could be identified beneath these artifacts (2–3 Hz for patient 9, and 10–20 Hz for patient 10). In order to enhance source localization methods, a bandpass filter was applied around the frequency of the discharges. Source localization results were difficult to interpret because the first visible scalp discharge to be analyzed may not be the initial discharge of the seizure. For patient 9, all source localization methods were concordant with SEEG (i.e. localized in the basal and medial parts of the left frontal lobe), whereas for patient 10 only ECD gave a concordant localization (i.e. localized in the left superior frontal sulcus). Although source localization methods gave concordant results, the goodness of fit was low. By comparison with other patients with the same signal to noise ratio, it was observed that artifacts decreased the goodness of fit of ECD models. These could be enhanced by signal preprocessing such as source separation (Levan et al., 2006).

Dynamic analysis of seizures

Across the different ictal patterns, two distinct situations were observed concerning the stability of source localizations. These situations were always the same with both the dipolar and distributed source models. The first situation was the reproducibility of source localization in the time window of analysis and in the successive ictal pattern of the seizure. It was observed that source localization methods can be applied to both the first pattern of the seizure and to the successive patterns of a seizure (from seizure onset to 3 s later). Reproducibility of the source localizations was a function of the signal to noise ratio. When this ratio was low, a displacement of the source model was often observed which corresponded to an invalid source model and not to anatomic propagation. An influence of signal to noise ratio was also observed during the time window of the ictal pattern. At the middle of the temporal window, which corresponded to the part of the signal with the maximum ratio, very stable source localizations were always observed (Gavaret et al., 2004). When ictal

Fig. 3. Scalp and depth electroencephalography (EEG), source localization, and stereoelectroencephalography (SEEG) schema for patient 7 (paroxysmal fast activity group). (A) Scalp-EEG ictal pattern was recorded over the right temporal region, the maximum amplitude being on channels F8, FT8 and FT10 (monopolar montage, common average reference). Scalp seizure onset is indicated with an arrow. Source localization methods were done on all events marked with a brace but only the source localization result of the ictal event marked with a triangle is presented. (B) Ictal source localizations in axial and frontal views. Rotating dipole, moving dipole, MUSIC, LORETA and sLORETA localizations are presented. All source localizations were located in the anterior and lateral part of the right temporal lobe. (C) Spatio-temporal analysis of the paroxysmal fast activity. Multiple rotating dipoles were calculated for three successive temporal windows (marked with a red, green, and blue brace). Two different localizations were observed: the first group of rotating dipoles (for red and blue braces) was in the lateral posterior part of the temporal lobe (red and blue circles on magnetic resonance image) whereas the second group (for green brace) was in the anterior part of the temporal lobe (green circle on magnetic resonance image). (D) SEEG schema, superimposed on patient's 3D magnetic resonance image was performed using eight depth electrodes in the right hemisphere and one in the left, recordings as follows (medial and lateral contacts): A, amygdala/anterior part of the middle temporal gyrus; B, hippocampal head/middle temporal gyrus; C, hippocampal tail/posterior part of middle temporal gyrus; T, superior temporal sulcus/anterior part of superior temporal gyrus; TP, posterior part of schizencephaly; D, posterior part of schizencephaly/temporo-parieto-occipital junction; O, posterior part of cingulate gyrus/posterior part of schizencephaly; TB, entorhinal cortex/inferior temporal gyrus; B', hippocampal head/anterior part of the middle temporal gyrus. (E) A strikingly similar ictal pattern was observed on intracerebral and surface EEG. Depth initial fast low-voltage discharge was recorded in the lateral temporal structures and involved not only the anterior part of the schizencephaly (C, middle contacts) but also the superior, middle and inferior temporal gyri (T, A, B, C, TB external contacts) and the anterior bank of the posterior schizencephaly (seizure onset is indicated with an arrow).

patterns were spike-like, an agreement between interictal and ictal source models seemed to give the best results. The only pattern that could not be localized was a flattening pattern, which corresponds to an activity $\leq 10 \mu\text{V}$ in amplitude (Foldvary et al., 2001). For patient 2, ictal spikes were followed by a diffuse flattening. Source localization on this flattening was not concordant with the fast discharge observed on intracerebral recording. The second situation concerning the stability of source localizations was the displacement of the source model in the epileptogenic network defined by SEEG. This rare observation was noted only for patient 7. A displacement of the source model was observed during the temporal window of analysis. Source models moved into the epileptogenic network, from the posterior to the anterior part of the temporal lobe, defined by SEEG. This displacement did not correspond to anatomic propagation of the generator but rather to the identification of the complete epileptogenic network identified by SEEG (anterior and lateral part of the right temporal lobe). Finally, it was interesting to note that spatio-temporal analysis for this patient enabled us to identify the entire epileptogenic network and thus the anatomic limit of this network.

In conclusion, a high level of agreement between source localization methods and SEEG can be obtained for ictal spike patterns and for scalp-EEG paroxysmal fast activities whereas scalp rhythmic discharges can be accurately localized but originated from seizure propagation network. All types of scalp ictal patterns can be accurately localized when they fulfill the following electrophysiologic requirements: for ictal spikes and rhythmic discharge patterns, a high value (>2) for the signal to noise ratio is necessary. The window of analysis should be free of artifacts (ocular, muscular, movements, notch, etc.). Furthermore, the time window of analysis should be at least 100 ms, especially for distributed source models. In contrast, ECD and MUSIC give accurate source localizations whatever the duration of the temporal window. All frequencies of scalp ictal patterns could be accurately localized. This localization sometimes needed bandpass filtering.

It will be interesting in the future to evaluate these source localization methods after preprocessing analysis of obscured ictal patterns. Finally, all types of epilepsy can be investigated by ictal HR-EEG. Further prospective studies are needed to assess the reliability and specificity of HR-EEG combined with source localization methods to localize the origin of scalp ictal discharges and to study their spatial relationship with the epileptogenic zone. Strangely, most ictal source localization studies have been done using MEG, despite the ergonomic constraints and short duration of acquisition. HR-EEG offers the possibility of recording seizures and performing precise ictal source localization in cases of ictal spike patterns and scalp-EEG paroxysmal fast activities whereas scalp rhythmic discharges can be accurately localized but originated from the seizure propagation network.

Acknowledgments

LK was supported by France Maintenance Biomedical and the French Ministry of Health (PHRC 17-05, 2009). The authors thank Prof. J. Regis, Prof. J.C. Peragut (Marseille), and Prof. J. Auque and Dr. S. Colnat-Coulbois (Nancy) for their neurosurgical contributions. The authors also thank P. Marquis for HR-EEG and SEEG data management.

Appendix A. Supplementary data

Supplementary data associated with this article can be found, in the online version, at doi:10.1016/j.neuroimage.2010.02.067.

References

Assaf, B., Ebersole, J., 1997. Continuous source imaging of scalp ictal rhythms in temporal lobe epilepsy. *Epilepsia* 38, 1114–1123.

- Azar, N.J., Lagrange, A.H., Abou-Khalil, B.W., 2009. Transitional sharp waves at ictal onset—a neocortical ictal pattern. *Clin. Neurophysiol.* 120 (4), 665–672.
- Bartolomei, F., Chauvel, P., Wendling, F., 2008. Epileptogenicity of brain structures in human temporal lobe epilepsy: a quantified study from intracerebral EEG. *Brain* 131, 1818–1830.
- Beniczky, S., Oturai, P.S., Alving, J., Sabers, A., Herning, M., Fabricius, M., 2006. Source analysis of epileptic discharges using multiple signal classification analysis. *Neuroreport* 17, 1283–1287.
- Blanke, O., Lantz, G., Seeck, M., Spinelli, L., Grave de Peralta, R., Thut, G., Landis, T., Michel, C.M., 2000. Temporal and spatial determination of EEG-seizure onset in the frequency domain. *Clin. Neurophysiol.* 111, 763–772.
- Boon, P., D'Have, M., Vandekerckhove, T., Achten, E., Adam, C., Clemenceau, S., Baulac, M., Goossens, L., Calliauw, L., De Reuck, J., 1997. Dipole modelling and intracranial EEG recording: correlation between dipole and ictal onset zone. *Acta Neurochir. (Wien)* 139, 643–652.
- Boon, P., D'Havé, M., Vanrumste, B., Van Hoey, G., Vonck, K., Van Walleghe, P., Caemaert, J., Achten, E., De Reuck, J., 2002. Ictal source localization in presurgical patients with refractory epilepsy. *J. Clin. Neurophysiol.* 19, 461–468.
- Bullmore, E.T., Brammer, M.J., Bourlon, P., Alarcon, G., Polkey, C.E., Elwes, R., Binnie, C.D., 1994. Fractal analysis of electroencephalographic signals intracerebrally recorded during 35 epileptic seizures: evaluation of a new method for synaptic visualisation of ictal events. *Electroencephalogr. Clin. Neurophysiol.* 91, 337–345.
- Chatrian, G.E., Bergamini, L., Dondey, M., Klass, D.W., Lennox-Buctal, M., Petersen, I., 1974. A glossary of terms most commonly used by clinical electroencephalographers. *Electroencephalogr. Clin. Neurophysiol.* 37, 538–548.
- Ding, L., Worrell, G.A., Lagerlund, T.D., He, B., 2007. Ictal source analysis: localization and imaging of causal interactions in humans. *Neuroimage* 34, 575–586.
- Ebersole, J.S., 2000. Noninvasive localization of epileptogenic foci by EEG source modeling. *Epilepsia* 41, 24–33.
- Eliashiv, D.S., Elsas, S.M., Squires, K., Fried, I., Engel Jr., J., 2002. Ictal magnetic source imaging as a localizing tool in partial epilepsy. *Neurology* 59, 1600–1610.
- Fischer, M.J., Scheler, G., Stefan, H., 2005. Utilization of magnetoencephalography results to obtain favourable outcomes in epilepsy surgery. *Brain* 128, 153–157.
- Foldvary, N., Klem, G., Hammel, J., Bingaman, W., Najm, I., Ludes, H., 2001. The localizing value of ictal EEG in focal epilepsy. *Neurology* 57, 2022–2028.
- Franaszczuk, P.J., Bergey, G.K., Kaminski, M.J., 1994. Analysis of mesial temporal seizure onset and propagation using the directed transfer function method. *Electroencephalogr. Clin. Neurophysiol.* 91, 413–427.
- Franaszczuk, P.J., Bergey, G.K., Durka, P.J., Eisenberg, H.M., 1998. Time-frequency analysis using the matching pursuit algorithm applied to seizures originating from the mesial temporal lobe. *Electroencephalogr. Clin. Neurophysiol.* 106, 513–521.
- Fuchs, M., Wagner, M., Kastner, J., 2004. Confidence limits of dipole source reconstruction results. *Clin. Neurophysiol.* 115, 1442–1451.
- Gavaret, M., Badier, J.M., Marquis, P., Bartolomei, F., Chauvel, P., 2004. Electric source imaging in temporal lobe epilepsy. *J. Clin. Neurophysiol.* 21, 267–282.
- Gavaret, M., Badier, J.M., Marquis, P., McGonigal, A., Bartolomei, F., Regis, J., Chauvel, P., 2006. Electric source imaging in frontal lobe epilepsy. *J. Clin. Neurophysiol.* 23, 358–370.
- Gavaret, M., Trébouchon, A., Bartolomei, F., Marquis, P., McGonigal, A., Wendling, F., Regis, J., Badier, J.M., Chauvel, P., 2009. Source localization of scalp-EEG interictal spikes in posterior cortex epilepsies investigated by HR-EEG and SEEG. *Epilepsia* 50, 276–289.
- Gonçalves, S., de Munck, J.C., Heethaar, R.M., Lopes da Silva, F.H., van Dijk, B.W., 2000. The application of electrical impedance tomography to reduce systematic errors in the EEG inverse problem: a simulation study. *Physiol. Meas.* 21, 379–393.
- Hilfiker, P., Egli, M., 1992. Detection and evolution of rhythmic components in ictal EEG using short segment spectra and discriminant analysis. *Electroencephalogr. Clin. Neurophysiol.* 82, 255–265.
- Holmes, M., Brown, M., Tucker, D., 2004. Are “generalized” seizures truly generalized? Evidence of localized mesial frontal and frontopolar discharges in absence. *Epilepsia* 45, 1568–1579.
- Knowlton, R.C., Elgavish, R., Howell, J., Blount, J., Burneo, J.G., Faught, E., Kankirawatana, P., Riley, K., Morawetz, R., Worthington, J., Kuzniecky, R.I., 2006. Magnetic source imaging versus intracranial electroencephalogram in epilepsy surgery: a prospective study. *Ann. Neurol.* 59, 835–842.
- Knowlton, R.C., Razdan, S.N., Limdi, N., Elgavish, R.A., Killen, J., Blount, J., Burneo, J.G., Ver Hoef, L., Paige, L., Faught, E., Kankirawatana, P., Bartolucci, A., Riley, K., Kuzniecky, R., 2009. Effect of epilepsy magnetic source imaging on intracranial electrode placement. *Ann. Neurol.* 65, 716–723.
- Koessler, L., Benhadid, A., Maillard, L., Vignal, J.P., Vespignani, H., Braun, M., 2008. Automatic localization of new scalp-recorded EEG sensors in MRI volume. *NeuroImage* 41, 914–923.
- Kuzniecky, R.I., Barkovich, A.J., 2001. Malformations of cortical development and epilepsy. *Brain Dev.* 23, 2–11.
- Lantz, G., Michel, C.M., Seeck, M., Blanke, O., Landis, T., Rosén, I., 1999. Frequency domain EEG source localization of ictal epileptiform activity in patients with partial complex epilepsy of temporal lobe origin. *Clin. Neurophysiol.* 110, 176–184.
- Lantz, G., Michel, C.M., Seeck, M., 2001. Characterisation of epileptiform EEG-activity during epileptic seizures, using space oriented segmentation and 3-dimensional source reconstruction. *Clin. Neurophysiol.* 112, 687–696.
- Lantz, G., Spinelli, L., Seeck, M., Grave de Peralta, R., Sottas, C., Michel, C., 2003. Propagation of interictal epileptiform activity can lead to erroneous source localizations: a 128-channel EEG mapping study. *J. Clin. Neurophysiol.* 20, 311–319.
- Lehnertz, K., Elger, C.E., 1995. Spatio-temporal dynamics of the primary epileptogenic area in temporal lobe epilepsy characterized by neuronal complexity loss. *Electroencephalogr. Clin. Neurophysiol.* 95, 108–117.

- LeVan, P., Urrestarazu, E., Gotman, J., 2006. A system for automatic artifact removal in ictal scalp EEG based on independent component analysis and Bayesian classification. *Clin. Neurophysiol.* 117, 912–927.
- Maillard, L., Koessler, L., Colnat-Coulbois, S., Vignal, J.-P., Louis-Dorr, V., Marie, P.-Y., 2009. Combined SEEG and source localisation study of temporal lobe schizencephaly and polymicrogyria. *Clin. Neurophysiol.* 120 (9), 1628–1636.
- Merlet, I., Gotman, J., 2001. Dipole modeling of scalp electroencephalogram epileptic discharges: correlation with intracerebral fields. *Clin. Neurophysiol.* 112, 414–430.
- Michel, C.M., Lehmann, D., Henggeler, B., Brandeis, D., 1992. Localization of the sources of EEG delta, theta, alpha and beta frequency bands using the FFT dipole approximation. *Electroencephalogr. Clin. Neurophysiol.* 82, 38–44.
- Michel, C., Lantz, G., Spinelli, L., Grave de Peralta, R., Landis, T., Seeck, M., 2004a. 128-channel EEG source imaging in epilepsy: clinical yield and localization precision. *J. Clin. Neurophysiol.* 21, 71–83.
- Michel, C.M., Murray, M.M., Lantz, G., Gonzalez, S., Spinelli, L., Grave de Peralta, R., 2004b. EEG source imaging. *Clin. Neurophysiol.* 115, 2195–2222.
- Mine, S., Yamaura, A., Iwasa, H., Nakajima, Y., Shibata, T., Itoh, T., 1998. Dipole source localization of ictal epileptiform activity. *Neuroreport* 9, 4007–4013.
- Mine, S., Iwasa, H., Kasagi, Y., Yamaura, A., 2005. Ictal dipole source analysis based on a realistic scalp–skull–brain head model in localizing the epileptogenic zone. *Neurosci. Res.* 51 (4), 453–461.
- Mosher, J.C., Baillet, S., Leahy, R.M., 1999. EEG source localization and imaging using multiple signal classification approaches. *J. Clin. Neurophysiol.* 16, 225–238.
- Oostendorp, T.F., Delbeke, J., Stegeman, D.F., 2000. The conductivity of the human skull: results of in vivo and in vitro measurements. *IEEE Trans. Biomed. Eng.* 47 (11), 1487–1492.
- Oostenveld, R., Praamstra, P., 2001. The five percent electrode system for high resolution EEG and ERP measurements. *Clin. Neurophysiol.* 112, 713–719.
- Osorio, I., Frei, M.G., Wilkinson, S.B., 1998. Real-time automated detection and quantitative analysis of seizures and short term prediction of clinical onset. *Epilepsia* 39, 615–627.
- Pascual-Marqui, R.D., 2002. Standardized low resolution brain electromagnetic tomography (sLORETA): technical details. *Method findings. Exp. Clin. Pharmacol.* 24D, 5–12.
- Pascual-Marqui, R.D., Michel, C.M., Lehmann, D., 1994. Low resolution electromagnetic tomography: a new method for localizing electrical activity in the brain. *Int. J. Psychophysiol.* 18, 49–65.
- Scherg, M., 1990. Fundamentals of dipole source potential analysis. In: Grandori, F., Hoke, M., Romani, G.L. (Eds.), *Auditory Evoked Electric and Magnetic Fields*. Karger, Basel, pp. 40–69.
- Schmidt, R.O., 1986. Multiple emitter location and signal parameter estimation. *IEEE Trans. Antennas Propag.* 34, 276–280.
- Stefan, H., Schneider, S., Feistel, H., Pawlik, G., Schüller, P., Abraham-Fuchs, K., Schlegel, T., Neubauer, U., Huk, W.J., 1992. Ictal and interictal activity in partial epilepsy recorded with multichannel magnetoencephalography: correlation of electroencephalography–electrocorticography, magnetic resonance imaging, single photon emission computed tomography and positron emission tomography findings. *Epilepsia* 33, 874–887.
- Stefan, H., Hummel, C., Scheler, G., Genow, A., Druschky, K., Tilz, C., Kaltenhäuser, M., Hopfengartner, R., Buchfelder, M., Romstock, J., 2003. Magnetic brain source imaging of focal epileptic activity: a synopsis of 455 cases. *Brain* 126, 2396–2405.
- Sutherling, W.W., Crandall, P.H., Engel Jr., J., Darcey, T.M., Cahan, L.D., Barth, D.S., 1987. The magnetic field of complex partial seizures agrees with intracranial localizations. *Ann. Neurol.* 21, 548–558.
- Talairach, J., Bancaud, J., 1966. Lesion, “irritative” zone and epileptogenic focus. *Confin. Neurol.* 27, 91–94.
- Talairach, J., Bancaud, J., Szikla, G., Bonis, A., Geier, S., Vedrenne, C., 1974. New approach to the neurosurgery of epilepsy. Stereotaxic methodology and therapeutic results. *Neurochirurgie* 20, 1–240.
- Tanaka, N., Cole, A.J., von Pechmann, D., Wakeman, D.G., Hämäläinen, M.S., Liu, H., et al., 2009. Dynamic statistical parametric mapping for analyzing ictal magnetoencephalographic spikes in patients with intractable frontal lobe epilepsy. *Epilepsy Res.* 85, 279–286.
- Trujillo-Barreto, N.J., Aubert-Vasquez, E., Valdez-Sosa, P.A., 2004. Bayesian model averaging in EEG/MEG imaging. *Neuroimage* 21 (4), 1300–1319.
- Unser, M., Aldroubi, A., 1996. A review of wavelets in biomedical applications. *Proc. IEEE* 84, 626–638.
- Worrell, G.A., Lagerlund, T.D., Sharbrough, F.W., Brinkmann, B.H., Busacker, N.E., Cicora, K.M., O'Brien, T.J., 2000. Localization of the epileptic focus by low-resolution electromagnetic tomography in patients with a lesion demonstrated by MRI. *Brain Topogr.* 12, 273–282.